NUMERICAL ANALYSIS OF TWO ENSEMBLE EDDY VISCOSITY MODELS OF FLUID MOTION

NAN JIANG AND WILLIAM LAYTON

Abstract. This report extends a recent method that calculates an ensemble of solutions of the Navier-Stokes equations efficiently to higher Reynolds number flows. To do so herein we develop and analyze two ensemble eddy viscosity models that do not obviate the good algorithmic properties of the ensemble method. The combined approach of ensemble time stepping and ensemble eddy viscosity modelling has other significant advantages. The form of the ensemble algorithm allows a new (and more accurate) parameterization of the turbulent viscosity coefficient that is more direct and gives an unconditionally stable algorithm. It also suggests a new definition of the mixing length. This new mixing length gives superior predictions of flows in our preliminary tests.

1. Introduction

In the numerical simulation of flows at higher Reynolds numbers (Re), incomplete data, quantification of uncertainty, increasing forecasting skill, quantification of flow sensitivities and other issues, e.g., [6], [12], [25], [28], [30], [31], [37], lead to the problem of computing ensembles, u_j, p_j, of solutions of the Navier-Stokes equations (**NSE**):

$$
\begin{aligned}
&u_{j,t} + u_j \cdot \nabla u_j - \nu \triangle u_j + \nabla p_j = f_j(x,t), \text{ in } \Omega,\ j = 1, ..., J \\
&\nabla \cdot u_j = 0, \text{ and } u_j(x,0) = u_j^0(x), \text{ in } \Omega \text{ and } u_j = 0, \text{ on } \partial\Omega.
\end{aligned} \tag{1.1}
$$

This leads to the competing demands of computing ensembles of solutions vs. the high resolution required for reliable simulations, [16]. One approach is to run a flow code J times in parallel, decreasing the available memory for each realization by a factor of J. Another approach, when available memory is consumed by the required resolution, is J sequentially runs, increasing turn-around time by a multiplier of J. In [21] a third possibility was advanced with complementary advantages and disadvantages of computing an ensemble of J solutions in one run. In this approach, the storage of vectors (but not matrices) used by the code is increased by a multiplier J. While the method is still relatively unexplored, storage required and turn around times may be reduced substantially over the first two alternatives. Indeed, the method (1.3) is linearly implicit. After spacial discretization, each time step requires the solution of one linear system with the same, shared coefficient matrix for each

Date: June 2013.
2000 *Mathematics Subject Classification.* Primary 65M12; Secondary 65J08 .
Key words and phrases. NSE, ensemble calculation, UQ.
The research herein was partially supported by NSF grant DMS 1216465 and Air Force grant FA 9550-12-1-0191.

ensemble member:

$$A\begin{bmatrix} u_1 & \cdots & u_J \\ p_1 & \cdots & p_J \end{bmatrix} = [RHS_1 | \cdots | RHS_J]. \tag{1.2}$$

This form allows the use of special projective, [9], or block iterative methods, e.g., [32], [10], [1], [8], [10], [11], [1] reducing the work required to advance in time[1].

The method of [21] without any parametrizations of turbulence requires a timestep condition $C\frac{\Delta t}{\nu \triangle x}\|\nabla u'\|^2 \leq 1$ that begins mild but degrades quickly as Re increases and fluctuations grow. This behavior has been reported for other methods, e.g. [26], and is exactly as expected for a method not incorporating a turbulence model. Herein, we extend (and analyze) the method to include two new ensemble eddy viscosity (**EEV**) type turbulence models with turbulent viscosity parametrizations

$$\textbf{EEV1:} \quad \nu_T = \mu_1 \triangle x |u'|, \quad \text{and}$$
$$\textbf{EEV2:} \quad \nu_T = \mu_2 |u'|^2 \triangle t.$$

These are based on direct parameterization of the energy in the turbulent fluctuations, $\frac{1}{2}|u'|^2$ and developed in Section 3. We also give, using the ensemble algorithm, *a redefinition of the LES lengthscale* from (the usual) $l = \triangle x$ to

$$l = \textit{ distance a fluctuating eddy travels in one time step} = |u'|\triangle t.$$

Our preliminary tests indicate that this change results in a model that is more stable numerically and less likely to over-diffuse the flow.

The precise analytical understanding of how the additional EEV term affects stability of the ensemble computation is an essential step in the development of the ensemble methods. The analysis in Section 4 delineates its positive effect; Algorithm (1.3) with EEV2 can be unconditionally stable, Theorem 1, Section 4.

1.1. **Methods and Models.** The euclidean length of a vector and Frobenius norm of an array is $|\cdot|$. The symmetric part of the velocity gradient tensor is denoted ∇^s. The ensemble mean $< u >$, fluctuation u'_j, its magnitude $|u'|$ and the induced kinetic energy density k' are

$$\text{mean: } < u >:= \frac{1}{J}\sum_{j=1}^{J} u_j, \text{ fluctuation: } u'_j := u_j - < u > ,$$

$$|u'|^2 := \sum_{j=1}^{J} |u'_j|^2 \text{ and energy density: } \; k' = \frac{1}{2}\,|u'|^2(x,t).$$

To present the method, suppress the secondary spacial discretization and let superscripts denote the timestep number. Thus, for example, $< u >^n, u'^n_j$ denote respectively approximations to $\frac{1}{J}\sum_{j=1}^{J} u_j(\cdot, t_n)$ and $u_j(\cdot,t_n) - < u >^n$ where $t_n := n\triangle t$. Consider the method: for $\quad j = 1, ..., J, \; \nabla \cdot u_j^{n+1} = 0, \;$ and

[1]To have a fixed matrix A (not changing from one time step to the next) would require lagging the entire nonlinear term. Since $Re \simeq |Nonlinear\ term| \;/\; |Viscous\ term|$, requiring the viscous term alone to control the lagged (and dominant as Re increases) nonlinear term leads to a severe time step restriction, [26].

$$
\begin{aligned}
(1.3) \qquad & \frac{u_j^{n+1}-u_j^n}{\Delta t} + < u >^n \cdot \nabla u_j^{n+1} + (u_j^n - < u >^n) \cdot \nabla u_j^n \\
& + \nabla p_j^{n+1} - \nu \Delta u_j^{n+1} - \nabla \cdot (\nu_T(l^n, k'^n) \nabla^s u_j^{n+1}) = f_j^{n+1}.
\end{aligned}
$$

The ensemble eddy viscosity parameterization is the coefficient $\nu_T(\cdot)$. Briefly, the Kolmogorov-Prandtl relation gives

$$
\begin{aligned}
\nu_T(\cdot) &= Const.l\sqrt{k'} \\
l &= \text{ mixing length of fluctuations,} \\
k' &= \text{ kinetic energy in fluctuations.}
\end{aligned}
$$

Often extensive (and optimistic) modelling steps are needed to generate representations of these two quantities, e.g., [34], [29]. Algorithm (1.3) allows direct calculation of both:

$$
k' = \frac{1}{2}|u'|^2 \text{ and } l = \begin{cases} \text{either } \triangle x, \\ \text{or } |u'|\triangle t \end{cases}.
$$

2. Notation and preliminaries

Let Ω be an open, regular domain in $\mathbb{R}^d$ ($d = 2$ or 3). The $L^2(\Omega)$ norm and the inner product are $\|\cdot\|$ and $(\cdot,\cdot)$. Likewise, the $L^p(\Omega)$ norms and the Sobolev $W_p^k(\Omega)$ norms are $\|\cdot\|_{L^p}$ and $\|\cdot\|_{W_p^k}$ respectively. $H^k(\Omega)$ is the Sobolev space $W_2^k(\Omega)$, with norm $\|\cdot\|_k$. Let X, Q, V denote the velocity, pressure and divergence free velocity spaces:

$$
\begin{aligned}
X &:= (H_0^1(\Omega))^d, \; Q := L_0^2(\Omega), \\
V &:= \{v \in X \; : (\nabla \cdot v, q) = 0 \; , \forall q \in Q\}.
\end{aligned}
$$

For $v \in X$ the usual $H^{1/2}(\Omega)$ norm satisfies the interpolation inequality

$$
\|v\|_{1/2} \leq C\sqrt{\|v\|\|\nabla v\|}.
$$

A weak formulation of (1.1) is: Find $u_j : [0,T] \to X$, $p_j : [0,T] \to Q$ satisfying, for $j = 1, ..., J$:

$$
\begin{gathered}
(u_{j,t}, v) + (u_j \cdot \nabla u_j, v) + \nu(\nabla u_j, \nabla v) - (p_j, \nabla \cdot v) = (f_j, v) \; , \forall v \in X \\
u_j(x, 0) = u_j^0(x) \text{ in } X \text{ and } (\nabla \cdot u_j, q) = 0, \forall q \in Q.
\end{gathered}
$$

Define $b(u,v,w) = (u \cdot \nabla v, w)$ and $b^*(u,v,w) := \frac{1}{2}(u \cdot \nabla v, w) - \frac{1}{2}(u \cdot \nabla w, v)$. By the divergence theorem

$$
b^*(u,v,w) = \int_\Omega u \cdot \nabla v \cdot w \; dx + \frac{1}{2}\int_\Omega (\nabla \cdot u)(v \cdot w) \; dx \tag{2.1}
$$

Both $b(\cdot,\cdot,\cdot)$ and $b^*(\cdot,\cdot,\cdot)$ satisfy: in both 3d and 2d (improvable in 2d)

$$
|b(u,v,w)| \text{ and } |b^*(u,v,w)| \leq C(\Omega)\|u\|_{1/2}\|\nabla v\|\|\nabla w\|.
$$

C represents a positive constant independent of ν, the solution u, the time step Δt and the mesh width h. Its value may vary from situation to situation.

2.1. **Finite Element Notation, Spaces and Formulation.** Conforming velocity, pressure finite element spaces based on an edge to edge triangulation of Ω (with maximum triangle diameter h) are denoted

$$X_h \subset X \;= (H_0^1(\Omega))^d,\, Q_h \subset Q = L_0^2(\Omega).$$

We assume that X_h and Q_h satisfy the usual discrete inf-sup condition. Taylor-Hood elements, e.g., [5], [13], are one choice used in the test in Section 6. The discretely divergence free subspace of X_h is

$$V_h \;:= \{v_h \in X_h : (\nabla \cdot v_h, q_h) = 0 \;,\, \forall q_h \in Q_h\}.$$

We assume finite element spaces satisfy standard inequalities (typical for quasi-uniform meshes, e.g., [5]), including: for all $v_h \in X_h$ and all elements e (with diameter h_e and minimum angle θ_e)

$$\text{(Inverse Ineq)} \qquad h_e \|\nabla v_h\|_{L^2(e)} \leq C(\theta_e)\|v_h\|_{L^2(e)},$$

$$\text{(Discrete Sobolev)} \qquad \|v_h\|_{L^\infty(\Omega)} \leq C|\ln h|^{1/2}\|\nabla v_h\|, \text{ in dimension } d = 2.$$

3. Ensemble Eddy Viscosity

The full development of EV models begins with local, spacial averaging followed by identifying the sub-filter scale stresses then replacing them by a term acting on the mean flow based on the eddy viscosity hypothesis / Boussinesq assumption that turbulent fluctuations are dissipative in the mean. These steps, carefully developed in, e.g., [3], [20], [22], [34], lead to an additional additive EV term:

$$-\nabla \cdot (2\nu_T(\cdot)\nabla^s u_j).$$

Since EV envisions turbulent fluctuations effects on the mean flow as a mixing process, $\nu_T(\cdot)$ must increase as the local kinetic energy density in the fluctuations increases. Phenomenology gives the Kolmogorov-Prandtl relation

$$\begin{aligned} \nu_T &= \nu_T(l, k') = \mu l \sqrt{k'} \\ l &= \text{ characteristic length scale of fluctuations,} \\ k' &= \text{ kinetic energy of the fluctuations,} \end{aligned}$$

or any dimensionally consistent relation involving the same variables.

Within the ensemble algorithm, the fluctuations about the mean can be directly computed rather than modelled. Accordingly, we take

$$k' = \sum_{j=1}^{J} \frac{1}{2}|u_j'|^2 := \frac{1}{2}|u'|^2.$$

For the characteristic length scale there are two natural and dimensionally correct choices:

$$\begin{aligned} l_1 &= \triangle x, \text{ after space discretization,} \\ l_2 &= |u'|\triangle t, \text{ for the considered time discretization.} \end{aligned}$$

The second relation, $l_2 = |u'|\triangle t$, expressed that the *characteristic length of turbulent fluctuations is the distance they travel in one time step.* We shall thus consider the parametrizations induced by these two length scales

$$\textbf{EEV1:}\quad \nu_T = \mu_1 \triangle x |u'|, \quad \text{and}$$
$$\textbf{EEV2:}\quad \nu_T = \mu_2 |u'|^2 \triangle t.$$

The mechanically correct form of the EEV above is in terms of the deformation tensor $\nabla^s u_j$. Since $\nabla \cdot u_j = 0$, this form is mathematically equivalent to one with the full gradient given by

$$-\nabla \cdot (\nu_T(l,k')\nabla u_j).$$

This form is also cheaper to implement in many codes. We shall therefore develop our theory for this latter form.

Ensemble averages equation: Taking the ensemble average of (1.3) gives a consistent discretization of the ensemble averaged NSE: $\nabla \cdot < u >^{n+1} = 0$ and

$$\frac{< u >^{n+1} - < u >^n}{\Delta t} + < u >^n \cdot \nabla < u >^{n+1} +$$
$$+ \left[< u_j^n \cdot \nabla u_j^n > - < u >^n \cdot \nabla < u >^n \right]$$
$$+\nabla < p >^{n+1} - \nu \Delta < u >^{n+1} - \nabla \cdot (\nu_T(l^n, k'^n)\nabla < u >^{n+1}) = < f >^{n+1}.$$

The term in brackets is the usual Reynolds stress term.

3.1. **Other ensemble eddy viscosity models.** We begin herein with simple and direct (while possibly not the most advanced) eddy viscosities. Others are possible; for example, parametrizations dimensionally consistent with EEV1&2, such as the following, are also consistent with the Kolmogorov-Prandtl relation:

$$\nu_T = \mu \triangle x^2 |\nabla^s u'|\ , \quad \mu |u'||\nabla^s u'| \triangle x \triangle t\ , \text{ and } \ \mu |\nabla^s u'|^2 \triangle t \triangle x^2.$$

Variational Multiscale Ensemble Eddy Viscosity. Variational multiscale methods (e.g., [19]) have proven to be powerful tools for turbulent flow simulations. The EEV parametrizations can be extended to ensemble variational multiscale models by

$$-\nabla \cdot (\nu_T(l,k')\nabla^s [u_j^{n+1} - < u >^{n+1}]).$$

This form preserves attractive features of the solution strategy. To be precise, consider the method: $\nabla \cdot u_j^{n+1} = 0$, and

$$\frac{u_j^{n+1} - u_j^n}{\Delta t} + < u >^n \cdot \nabla u_j^{n+1} + (u_j^n - < u >^n) \cdot \nabla u_j^n + \nabla p_j^{n+1}$$
$$-\nu \Delta u_j^{n+1} - \nabla \cdot (\nu_T(l,k')\nabla^s [u_j^{n+1} - < u >^{n+1}]) = f_j^{n+1}.$$

The linear system for the new time level takes the form

$$A_0 \begin{bmatrix} u_j^{n+1} \\ p_j^{n+1} \end{bmatrix} + A_1 \begin{bmatrix} \frac{1}{J}\sum_{j=1}^J u_j^{n+1} \\ \frac{1}{J}\sum_{j=1}^J p_j^{n+1} \end{bmatrix} = RHS_j, j = 1, \cdots, J,$$

where the matrices $A_{0/1}$ are independent of j (but depend on the timestep number n). Writing this as a coupled system for u_j^{n+1}, it becomes a fully coupled, block $J \times J$ system. To uncouple the system, solve for first $<u>^{n+1}$ and then $u_j'^{n+1} = u_j^{n+1} - < u >^{n+1}$. Note that

$$< \nabla \cdot (\nu_T(l,k')\nabla^s [u_j^{n+1} - < u >^{n+1}]) > =$$
$$\nabla \cdot (\nu_T(l,k')\nabla^s [< u_j^{n+1} > - < u >^{n+1}]) = 0.$$

Taking the ensemble mean thus eliminates the coupling:

$$A_0 \left[\begin{array}{c} < u >^{n+1} \\ < p >^{n+1} \end{array} \right] = < RHS_j > .$$

Subtracting shows that the fluctuations satisfy: for $j = 1, \cdots, J$

$$A_0 \left[\begin{array}{c} u_j'^{n+1} \\ p_j'^{n+1} \end{array} \right] = RHS_j - < RHS_j > - A_1 \left[\begin{array}{c} < u >^{n+1} \\ < p >^{n+1} \end{array} \right].$$

The solution procedure then consists of one linear system with coefficient matrix A_0 followed by J linear systems with A_0 as common coefficient matrix.

4. Stability of the Ensemble Eddy Viscosity Algorithm

Many spacial discretizations are used for flow problems. Thus we shall begin by studying stability of the discrete time, continuous space approximation which can be implemented by any common space discretization. Consider (1.3) where ν_T is given by

$$\begin{aligned} &\textbf{EEV1:} \quad \nu_T = \mu_1 \triangle x |u'|, \text{ or} \\ &\textbf{EEV2:} \quad \nu_T = \mu_2 |u'|^2 \triangle t. \end{aligned} \tag{4.1}$$

The stability analysis of Theorems $1-4$ below is based on energy methods (and without Gronwall's inequality). Thus it yields global, nonlinear, long time stability. For each variant we take $\sum_{j=1}^{J} \int_\Omega Method \cdot u_j^{n+1} dx$ and arrive at

$$E^{n+1} - E^n + \triangle t [D^{n+1} - N^{n+1}] = \triangle t P^{n+1},$$

where, at the indicated time, E = system energy, D = rate of viscous, numerical and eddy viscosity dissipation, N = nonlinear term, and P = energy input through body force - flow interactions. Long time, nonlinear stability thus follows provided $D^{n+1} \geq N^{n+1}$. The key step in the proofs will be to show the following, which suffices for stability,

$$\int_\Omega \left\{ 2[\nu + \nu_T(l^n, k'^n)] |\nabla u_j^{n+1}|^2 - \triangle t |u_j'^n|^2 |\nabla u_j^{n+1}|^2 \right\} dx \geq 0.$$

One striking result is unconditional stability for EEV2 when $\mu_2 \geq 1/2$, Theorem 1. In the spatially discrete case, stability requires control of $||\nabla \cdot u^{n+1}||$, Theorem 3. For EEV1, stability requires more: either an Re dependent timestep condition or a local timestep condition, Theorems $2, 4$ and 5.

The case of EEV2: $\nu_T = \mu_2 |u'|^2 \triangle t$.

Theorem 1 (Unconditional Stability of EEV2)**.** *The method (1.3) with EEV2 $\nu_T = \mu_2 |u'|^2 \triangle t$ is unconditionally, nonlinearly, long time stable (even for $\nu = 0$) if*

$$\mu_2 \geq \frac{1}{2}, \tag{4.2}$$

or if

$$\frac{\triangle t |u_j'^n|^2}{2\nu} \leq 1, \tag{4.3}$$

or if, for some $\theta, 0 \leq \theta \leq 1$, the timestep condition holds:

$$\mu_2 \geq \frac{\theta}{2}, \quad \textit{and} \quad (1-\theta) \frac{\triangle t |u_j'^n|^2}{2\nu} \leq 1. \tag{4.4}$$

Proof. Take the inner product of the equation with u_j^{n+1}. Multiplying by $2\triangle t$, using skew symmetry of the first nonlinear term and the polarization identity in the time difference term. This yields

$$||u_j^{n+1}||^2 - ||u_j^n||^2 + ||u_j^{n+1} - u_j^n||^2 + 2\triangle t\left((u_j^n - <u>^n) \cdot \nabla u_j^n, u_j^{n+1}\right) + \\ +2\triangle t \int_\Omega [\nu + \nu_T(l^n, k'^n)]|\nabla u_j^{n+1}|^2 dx = 2\triangle t\left(f_j^{n+1}, u_j^{n+1}\right).$$

By skew symmetry we have

$$\begin{aligned}\left((u_j^n - <u>^n) \cdot \nabla u_j^n, u_j^{n+1}\right) &= \left((u_j^n - <u>^n) \cdot \nabla u_j^n, u_j^{n+1} - u_j^n\right) = \\ &= \left((u_j^n - <u>^n) \cdot \nabla [u_j^n + u_j^{n+1} - u_j^n], u_j^{n+1} - u_j^n\right) \\ &= \left((u_j^n - <u>^n) \cdot \nabla u_j^{n+1}, u_j^{n+1} - u_j^n\right).\end{aligned}$$

Nonlinear, long time stability thus follows provided

$$||u_j^{n+1} - u_j^n||^2 + 2\triangle t \int_\Omega [\nu + \nu_T(l^n, k'^n)]|\nabla u_j^{n+1}|^2 dx + \\ +2\triangle t\left((u_j^n - <u>^n) \cdot \nabla u_j^{n+1}, u_j^{n+1} - u_j^n\right) \geq 0.$$

The first two terms are nonnegative and the third can have two signs. We thus consider the third term. We have

$$2\triangle t\left|\left((u_j^n - <u>^n) \cdot \nabla u_j^{n+1}, u_j^{n+1} - u_j^n\right)\right| \leq ||u_j^{n+1} - u_j^n||^2 + \triangle t^2 \int_\Omega |u_j'^n|^2 |\nabla u_j^{n+1}|^2 dx.$$

Using this as a worst case bound for the third term gives the sufficient condition

$$\int_\Omega \left\{2[\nu + \nu_T(l^n, k'^n)]|\nabla u_j^{n+1}|^2 - \triangle t |u_j'^n|^2 |\nabla u_j^{n+1}|^2\right\} dx \geq 0.$$

With the EV parameterization $\nu_T = \mu_2 |u'|^2 \triangle t$, this becomes

$$\int_\Omega [2\nu + \triangle t\left(2\mu_2 |u'^n|^2 - |u_j'^n|^2\right)]|\nabla u_j^{n+1}|^2 dx \geq 0,$$

from which the first stability result follows when $\mu_2 \geq \frac{1}{2}$, i.e., (4.2). For the second condition (4.3), noting that it makes no reference to the eddy viscosity term, stability under the second condition follows by absorbing the term $\triangle t|u'|^2|\nabla u|^2$ in the viscous term $2\nu|\nabla u|^2$ similarly. The third condition (4.4) is a simple combination of the first two. ∎

The case of EEV1: $\nu_T = \mu_1 \triangle x |u'|$. Following the proof of Theorem 1 and solving a quadratic inequality gives the following pointwise CFL condition for EEV1.

Theorem 2 (Conditional stability of EEV1)**.** *Consider (1.3) with the parameterization*

$$\textbf{\textit{EEV1}}\text{: } \nu_T = \mu_1 \triangle x |u'|.$$

A sufficient condition for stability is that there holds pointwise

$$\frac{\triangle t |u'(x, t_n)|}{\triangle x} \leq \frac{1}{2}\mu_1 + \sqrt{\left(\frac{1}{2}\mu_1\right)^2 + \frac{\nu \triangle t}{\triangle x^2}}. \tag{4.5}$$

This is implied by the two special cases

$$\frac{\triangle t |u'(x, t_n)|}{\triangle x} \leq \mu_1, \quad \textit{or} \quad \frac{\triangle t |u'(x, t_n)|^2}{\nu} \leq 1. \tag{4.6}$$

Proof. The proof for EEV2 was independent of the particular EEV parameterization until the last step. Inserting EEV1 gives the sufficient condition

$$\int_\Omega [2\nu + \left(2\mu_1 \triangle x|u'| - \triangle t|u_j'^n|^2\right)]|\nabla u_j^{n+1}|^2 dx \geq 0.$$

A sufficient condition for this is that the quadratic form $[2\nu + \left(2\mu_1 \triangle x|u'^n| - \triangle t|u'^n|^2\right)] \geq 0$. Let

$$s = \frac{\triangle t|u'^n|}{2\triangle x} \geq 0.$$

By rescaling, the following condition suffices for stability

$$\nu + 2\mu_1 \frac{\triangle x^2}{\triangle t} s - 2\frac{\triangle x^2}{\triangle t} s^2 \geq 0.$$

The first stability condition (4.5) follows by solving the quadratic inequality. The second condition (4.6) follow by dropping terms in the RHS. ∎

5. Stability : Discrete Space and Time

This section analyzes stability under spacial discretization by finite element methods; extension to other methods is both interesting and important. There are two essential deviations from the spatially continuous case. First, new options are available for analysis of stability: since the FEM spaces are finite dimensional, norm equivalence tools can be used and lead to CFL type timestep conditions involving the ratio $\triangle t/\triangle x$. Second, since common FEM velocity spaces are not exactly divergence free, new restrictions depending on the size of $||\nabla \cdot u_h||$ emerge from the nonlinear term. These are not active for Fourier spectral methods when using divergence free FEM spaces and suggest further study of the methods with grad-div stabilization, e.g., [33], [7], added. Similarly to the analysis in [27], these terms occur here from the nonlinearity rather than from the pressure-incompressibility coupling.

Since all velocities and pressures in this section are discrete we drop subscripts "h" on discrete velocities and pressures to simplify notation. The usual (no extra stabilization) fully discrete EEV FEM is: *Given* u_j^n, *find* $u_j^{n+1} \in X_h$, $p_j^{n+1} \in Q_h$ *satisfying*

$$\begin{aligned}
&(\frac{u_j^{n+1} - u_j^n}{\Delta t}, v) + b^*(< u >^n, u_j^{n+1}, v) + b^*(u_j^n - < u >^n, u_j^n, v) \\
&-(p_j^{n+1}, \nabla \cdot v) + ([\nu + \nu_T^n]\, \nabla u_j^{n+1}, \nabla v) = (f_j^{n+1}, v), \qquad \forall v \in X_h, \\
&(\nabla \cdot u_j^{n+1}, q) = 0, \qquad \forall q \in Q_h, \\
&u_j(0) \in X_h \text{ given.}
\end{aligned} \tag{5.1}$$

Theorem 3 (Stability)**.** *The method (5.1) with the parameterization* ***EEV2,*** $\nu_T = \mu_2 \triangle t|u'|^2$***,*** *is nonlinearly, long time stable if, for some* θ *and* α, $0 \leq \theta \leq 1$, $0 < \alpha < 1$, *the timestep condition holds,*

$$\theta\nu + 2\Delta t(\mu_2 - \frac{1}{2\alpha})|u_j'^n| \geq 0 \quad \textit{and} \quad (1-\theta)\nu - \frac{C}{4(1-\alpha)}\Delta t\|\nabla \cdot u_j'^n\|_{L^4}^2 \geq 0. \tag{5.2}$$

In particular, stability follows if

$$\nabla \cdot u_j'^n = 0 \textit{ and } \mu_2 > \frac{1}{2}.$$

Proof. We follow the proof of Theorem 1 to the divergence point. Set $v = u_j^{n+1}$, $q = p_j^{n+1}$ and multiply by $2\triangle t$. Using skew symmetry of $b^*(<u>^n, u_j^{n+1}, v)$ and the polarization identity in (u_j^n, u_j^{n+1}) in the time difference term gives

$$||u_j^{n+1}||^2 - ||u_j^n||^2 + ||u_j^{n+1} - u_j^n||^2 + 2\triangle t b^*\left(u_j'^n, u_j^{n+1}, u_j^{n+1} - u_j^n\right) + \\ +2\triangle t \int_\Omega [\nu + \nu_T(l^n, k'^n)] |\nabla u_j^{n+1}|^2 dx = 2\triangle t\left(f_j^{n+1}, u_j^{n+1}\right).$$

Applying Young's inequality to the right hand side gives

$$||u_j^{n+1}||^2 - ||u_j^n||^2 + ||u_j^{n+1} - u_j^n||^2 + 2\triangle t b^*\left(u_j'^n, u_j^{n+1}, u_j^{n+1} - u_j^n\right) + \\ +\triangle t \int_\Omega [\nu + 2\nu_T(l^n, k'^n)] |\nabla u_j^{n+1}|^2 dx \leq \frac{\triangle t}{\nu} \|f_j^{n+1}\|_*^2.$$

Using (2.1),

$$2\triangle t b^*\left(u_j'^n, u_j^{n+1}, u_j^{n+1} - u_j^n\right) = \\ 2\triangle t\left(u_j'^n \cdot \nabla u_j^{n+1}, u_j^{n+1} - u_j^n\right) + \triangle t\left(\nabla \cdot u_j'^n, u_j^{n+1} \cdot (u_j^{n+1} - u_j^n)\right).$$

For the two terms on the above RHS we have, for any $0 < \alpha < 1$,

$$\text{(Term 1)} \;\; 2\triangle t\left|\left(u_j'^n \cdot \nabla u_j^{n+1}, u_j^{n+1} - u_j^n\right)\right| \leq \\ \leq \alpha \|u_j^{n+1} - u_j^n\|^2 + \frac{\triangle t^2}{\alpha} \int_\Omega |u_j'^n|^2 |\nabla u_j^{n+1}|^2 dx, \\ \text{(Term 2)} \;\; \triangle t\left|\left(\nabla \cdot u_j'^n, u_j^{n+1} \cdot (u_j^{n+1} - u_j^n)\right)\right| \leq \\ \leq (1-\alpha)\|u_j^{n+1} - u_j^n\|^2 + \frac{\triangle t^2}{4(1-\alpha)} \int_\Omega |\nabla \cdot u_j'^n|^2 |u_j^{n+1}|^2 dx.$$

Inserting these bounds and EEV2 into the energy estimate, nonlinear, long time stability thus follows provided

$$\int_\Omega \{(\nu + 2\mu_2 \triangle t |u'^n|^2) |\nabla u_j^{n+1}|^2 \\ -\triangle t(\frac{1}{\alpha}|u_j'^n|^2 |\nabla u_j^{n+1}|^2 + \frac{1}{4(1-\alpha)} |\nabla \cdot u_j'^n|^2 |u_j^{n+1}|^2)\} dx \geq 0.$$

This follows provided, for some θ, $0 \leq \theta \leq 1$,

$$\int_\Omega \{[\theta\nu + 2\triangle t(\mu_2 - \frac{1}{2\alpha}) |u'^n|^2] |\nabla u_j^{n+1}|^2 \\ +[(1-\theta)\nu |\nabla u_j^{n+1}|^2 - \frac{1}{4(1-\alpha)} \triangle t |\nabla \cdot u_j'^n|^2 |u_j^{n+1}|^2]\} dx \geq 0. \tag{5.3}$$

(5.3) holds if

$$\theta\nu + 2\triangle t(\mu_2 - \frac{1}{2\alpha}) |u'^n|^2 \geq 0, \qquad \text{and} \\ (1-\theta)\nu \|\nabla u_j^{n+1}\|^2 - \frac{1}{4(1-\alpha)} \triangle t \|\nabla \cdot u_j'^n\|_{L^4}^2 \|u_j^{n+1}\|_{L^4}^2 \geq 0.$$

The Sobolev embedding theorem and the Poincaré inequality yield

$$\theta\nu + 2\triangle t(\mu_2 - \frac{1}{2\alpha})|u'^n|^2 \geq 0, \qquad \text{and}$$
$$(1-\theta)\nu\|\nabla u_j^{n+1}\|^2 - \frac{C}{4(1-\alpha)}\triangle t\|\nabla \cdot u_j'^n\|_{L^4}^2\|\nabla u_j^{n+1}\|^2 \geq 0,$$

which, completing the proof, are equivalent to (5.2). ∎

Next EEV1 is considered.

Theorem 4. *Consider (5.1) with EEV1 $\nu_T = \mu_1\triangle x|u'|$. A sufficient condition for stability is that if for some θ, $0 \leq \theta \leq 1$, the two timestep conditions hold,*

$$(5.4) \quad (1-\theta)\nu - \frac{C}{2}\Delta t\|\nabla \cdot u_j'^n\|_{L^4}^2 \geq 0, \quad \frac{\triangle t|u'(x,t_n)|}{\triangle x} \leq \frac{1}{2}\mu_1 + \frac{1}{2}\sqrt{\mu_1^2 + \frac{\theta\nu\triangle t}{\triangle x^2}}.$$

This is implied by the two special cases

$$(1-\theta)\nu - \frac{C}{2}\Delta t\|\nabla \cdot u_j'^n\|_{L^4}^2 \geq 0 \quad \textit{and} \quad \frac{\triangle t|u'(x,t_n)|}{\triangle x} \leq \frac{1}{2}\mu_1,$$
$$\textit{or} \quad (1-\theta)\nu - \frac{C}{2}\Delta t\|\nabla \cdot u_j'^n\|_{L^4}^2 \geq 0 \quad \textit{and} \quad \frac{\triangle t|u'(x,t_n)|^2}{\theta\nu} \leq \frac{1}{4}.$$

Proof. Following the proof of Theorem 3 with EEV1 gives the sufficient condition

$$\int_\Omega \{[\nu + 2\mu_1\triangle x|u'^n|]|\nabla u_j^{n+1}|^2$$
$$-\triangle t[2|u_j'^n|^2|\nabla u_j^{n+1}|^2 + \frac{1}{2}|\nabla \cdot u_j'^n|^2|u_j^{n+1}|^2]\}dx \geq 0.$$

This follows provided, for some θ, $0 \leq \theta \leq 1$,

$$(5.5) \qquad \int_\Omega \{[\theta\nu + 2\mu_1\triangle x|u'^n| - 2\triangle t|u'^n|^2]|\nabla u_j^{n+1}|^2$$
$$+[(1-\theta)\nu|\nabla u_j^{n+1}|^2 - \frac{1}{2}\triangle t|\nabla \cdot u_j'^n|^2|u_j^{n+1}|^2]\}dx \geq 0.$$

(5.5) holds if

$$\theta\nu + 2\mu_1\triangle x|u'^n| - 2\triangle t|u'^n|^2 \geq 0, \qquad \text{and}$$
$$(1-\theta)\nu\|\nabla u_j^{n+1}\|^2 - \frac{1}{2}\triangle t\|\nabla \cdot u_j'^n\|_{L^4}^2\|u_j^{n+1}\|_{L^4}^2 \geq 0.$$

Since $\|u\|_{L^4} \leq C(\Omega)\|\nabla u\|$, the stability conditions become

$$\theta\nu + 2\mu_1\triangle x|u'^n| - 2\triangle t|u'^n|^2 \geq 0, \qquad \text{and}$$
$$(1-\theta)\nu - \frac{C}{2}\triangle t\|\nabla \cdot u_j'^n\|_{L^4}^2 \geq 0.$$

Rescale by $s = \triangle t|u'^n|/\triangle x \geq 0$:

$$\theta\nu + 2\mu_1\frac{\triangle x^2}{\triangle t}s - 2\frac{\triangle x^2}{\triangle t}s^2 \geq 0.$$

Solving the quadratic inequality, we obtain (5.4). ∎

All the stability conditions can be applied locally when the $\triangle x$ in the model is the local meshwidth h_e, e.g.,

$$\begin{aligned}\frac{\triangle t|u'(x,t_n)|}{\triangle x} &\leq \frac{1}{2}\mu_1 \text{ replaced by}\\ \frac{\triangle t \max_{x\in e}|u'(x,t_n)|}{h_e} &\leq \frac{1}{2}\mu_1 \text{ for all elements } e.\end{aligned}$$

Finally, note that both EEV terms are nonnegative. Thus, stability follows from any of the conditions derived in [21] for the laminar case (where $\nu_T = 0$). We summarize these without proof.

Theorem 5 (Stability: laminar flow timestep conditions)**.** *Consider the method (5.1) with either EEV1 or EEV2. Stability holds under any of the conditions below (where $C = C(\Omega)$) for the indicated cases:*

$$C\frac{\Delta t}{\nu\triangle x}\|\nabla u_j'^n\|^2 \leq 1, \quad \textit{in 2d and 3d},$$

$$C\frac{|ln(h)|\Delta t}{\nu}\|\nabla u_j'^n\|^2 \leq 1, \quad \textit{in 2d},$$

$$C\frac{\Delta t}{\nu\triangle x^2}(\|u_j'^n\|^2 + \|\nabla\cdot u_j'^n\|^2) \leq 1, \quad \textit{in 2d},$$

$$C\frac{\Delta t}{\nu\triangle x^2}\|u_j'^n\|^2_{L^3} \leq 1, \; \textit{in 3d},$$

$$C\max_e \frac{\Delta t}{\nu h_e}\|\nabla u_j'^n\|^2_{L^2(e)} \leq 1, \quad \textit{in 3d on locally refined meshes.}$$

6. Numerical Tests

In tests in [21] with $\nu_T = 0$ it was seen clearly that as the Reynolds number increased, the timestep restriction imposed for stability, summarized in Theorem 5, forced the timestep to become exceedingly small. The main goal of these tests (performed using FreeFEM++, [17]) is to check the theoretical predictions of Theorems $1-4$ of the effect on stability of the added EEV terms. We thus begin with tests from [21] at the Reynolds numbers at which the laminar criteria failed. While these first tests are $2d$, they reveal interesting differences among the methods.

Test 1 was for *flow between offset cylinders* driven by a rotating body force ($Re = 800$). Space averaged statistics of interest to rotating flow were tracked in time. The ensemble method plus EEV2 yielded reasonable statistics, see Figures 2, 3, 4, 19, 21. Stability for EEV2 was obtained for moderate timesteps while no ensemble eddy viscosity ($\nu_T = 0$) required time adaptivity and prohibitively small timesteps, Figure 1 Left and Right. The noEV simulation also yielded nonsensical solutions (Supplementary Material).

One anomaly observed was that the time average *EEV2 kinetic energy was somewhat greater than that of the noEV solutions.* This was because the EEV2 solutions align more with the body force and thus there is more energy input through body force-flow interactions (through $2\triangle t(f^{n+1}, u^{n+1})$) that with the noEV solutions, due to cancellation in the nonphysical, $O(\triangle x)$ eddies, expected in under-resolved flows. **Test 2** compared EEV1 and EEV2 for the same geometry at $Re = 800, 1200, 2400$ and constant timestep $\triangle t = 0.025$. noEV runs failed at $Re = 1200, 2400$. *EEV2, while more stable numerically, gave better solutions than*

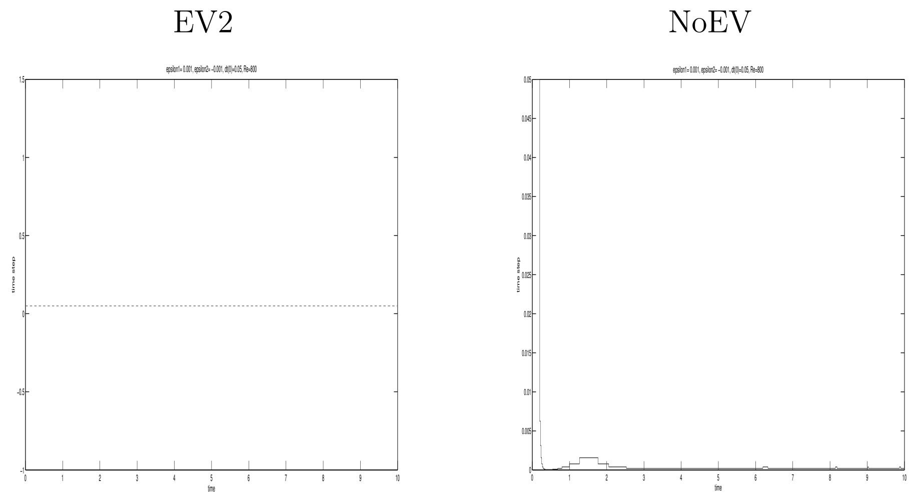

FIGURE 1. Timestep evolution, $\nu = 1/800$,

EEV1. Indeed, *EEV1 dramatically over-diffused the flow*; solutions very quickly approach nonphysical Stokes-flow like velocities. To improve EEV1 two possibilities are natural: a better choice of μ_1 and reinitialization of perturbations (Test 3). In exhaustive tests (not reported herein), we found the EEV1 solutions to be very sensitive to μ_1 with a narrow range of μ_1-values producing good results. This observation opens interesting research questions as yet unresolved. **Test 3** (results given in the supplementary materials) repeated these two tests but *reinitialized the perturbations* at $t = 1, 2, 3, \cdots$. The conclusions regarding stability were not altered by reinitialization. **Test 4** was an accuracy test with a smooth, known exact solution. In Test 4 *both EEV1 and EEV2 produced 2 significant digits of accuracy with* $\triangle x = 0.1$, an acceptable result. **Test 5** is a flow in a *channel with 2 outlets and a constriction* from [4, 18, 23]. Both EEV1 and EEV2 gave the correct general outlines of the flow (compared to a fine mesh solution presented in the Supplement and others published results) and differences in the smaller details of the flow.

Test 1: Stability of noEV vs. EEV2 for flow between offset circles. Motivated by the classic problem of flow between rotating cylinders, the domain is a disk with a smaller, off-center obstacle inside. Let $r_1 = 1$, $r_2 = 0.1$, $c = (c_1, c_2) = (\frac{1}{2}, 0)$. The domain and body force are given by

$$\Omega = \{(x, y) : x^2 + y^2 \leq r_1^2 \text{ and } (x - c_1)^2 + (y - c_2)^2 \geq r_2^2\},$$
$$f(x, y, t) = (-4y * (1 - x^2 - y^2), 4x * (1 - x^2 - y^2))^T$$

with no-slip boundary conditions on both circles. The flow, driven by a counterclockwise force with $f \equiv 0$ at the outer circle at $Re = 800$, rotates about $(0, 0)$ and interacts with the immersed circle $(x - c_1)^2 + (y - c_2)^2 \leq r_2^2$. This induces a von Kármán vortex street which re-interacts with the immersed circle creating more complex structures. The mesh has $n = 40$ mesh points around the outer circle and $m = 10$ mesh points around the immersed circle, and extended to Ω as a Delaunay mesh. This flow will be under-resolved. Thus we test stability of flow statistics but not flow details.

Adapting the timestep. For EEV2 and NoEV, we take the constant $C = 1/1200$. For EEV2, we take $\mu_2 = 1$ and adapt the timestep by halving and doubling to enforce (5.2):

$$0.5 * \frac{2400}{Re} \leq \Delta t ||\nabla \cdot (u_{j,h}^n - < u_h >^n)||_{L^4}^2 \leq \frac{2400}{Re}, \text{ subject to } \triangle t \leq 0.05.$$

For NoEV, similarly halving and doubling enforces the $2d$ condition of [21]

$$0.5 * \frac{1200}{Re} \leq |ln(h)| \Delta t ||\nabla (u_{j,h}^n - < u_h >^n)||^2 \leq \frac{1200}{Re}, \text{ subject to } \triangle t \leq 0.05.$$

The timestep evolution is in Figure 1. Without enforcing $\triangle t \leq 0.05$, EEV2 adaptivity increased $\triangle t$ to $\triangle t \geq 12$, suggesting that EEV2 also controls errors in $||\nabla \cdot u||$ and that the value $\mu_2 = 1$ could be further reduced significantly for this flow.

Generation of the initial conditions. Initial perturbations $u_j^0, j = 1, 2$, and u_0^0 (with $\epsilon \equiv 0$, 'no perturbation'), are generated by solving the steady Stokes problem with body forces perturbed by $\pm\epsilon(sin(3\pi x)sin(3\pi y), cos(3\pi x)cos(3\pi y))^T$. We choose $\epsilon = 10^{-3}$. These initial conditions give u_1, u_2, $u_{ave} = (u_1 + u_2)/2$ and u_0 (initial condition u_0^0 -'no perturbation').

Quantities plotted. We plot over $0 \leq t \leq 10$ *angular momentum*, *enstrophy*, *energy* (integral invariants of the Euler equations of relevance to rotational flows) and *total dissipation rates* for EEV2 and noEV:

$$|\text{Angular Momentum}| = |\int_\Omega \vec{x} \times \vec{u} \, d\vec{x}|, \qquad \text{Enstrophy} = \tfrac{1}{2}\nu \|\nabla \times \vec{u}\|^2,$$
$$\text{Energy} = \tfrac{1}{2}\|u\|^2, \qquad \text{Power Input} = \left(f_j^{n+1}, u_j^{n+1}\right),$$

$$\begin{aligned} \text{EEV2-Dissipation} &= \frac{1}{2\triangle t}\|u_j^{n+1} - u_j^n\|^2 + b^*\left(u_j'^n, u_j^n, u_j^{n+1}\right) \\ &\quad + \int_\Omega [\nu + \nu_T(\,\cdot\,)] |\nabla u_j^{n+1}|^2 dx, \\ \text{NoEV-Dissipation} &= \frac{1}{2\triangle t}\|u_j^{n+1} - u_j^n\|^2 + b^*\left(u_j'^n, u_j^n, u_j^{n+1}\right) \\ &\quad + \nu \|\nabla u_j^{n+1}\|^2. \end{aligned}$$

Next the Reynolds number was increased to $Re = 1200$ and 2400. At $Re = 1200$, 2400 the noEV runs failed while EEV2 remained stable with $\triangle t = 0.05$.

Test 2: Stability of EEV1 vs. EEV2. Test 1 was repeated comparing EEV1 and EEV2 for $Re = 800$ and constant timestep. We take $\Delta t = 0.025, Re = 800, \mu_2 = 1, \mu_1 \Delta x = 0.2$

The EEV1 simulation is clearly over-damped. The streamlines (Supplementary Material) of the EEV1 simulation show that the velocity has converged to the Stokes flow solution which is incorrect. Strong over-damping of EEV1 vs. EEV2 was a consistent result and was only corrected by a brute force search for an optimal EEV1 parameter.

Test #3: Re-initialization: If every ensemble member has the same body forces and slightly perturbed initial conditions, then over small time the fluctuations remain small and over intermediate time they may give a reasonable estimate of the kinetic energy in turbulent fluctuations. Over longer time, the trajectories determined by these nearby initial conditions separate and (while constrained to

EEV2

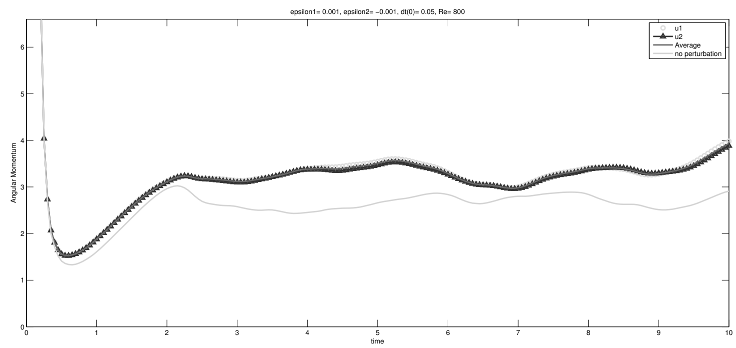

NoEV

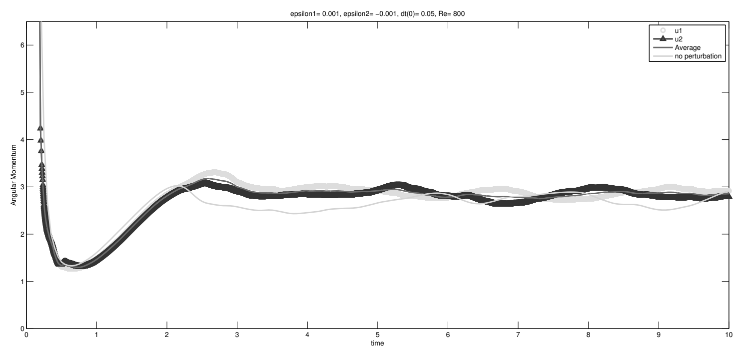

FIGURE 2. Angular Momentum, $\nu = 1/800$

the same ball in $L^{\infty}\ (0,T;L^2(\Omega\ )) \cap L^2\ (0,T;H^1(\Omega\ ))\ k' \to O(1)$. Periodic reinitialization of the ensembles may be necessary and may alter the conclusions of the tests. To check this, we repeat Test 2 but reinitialize the perturbation at $t = 1,2,3,\cdots$, restarting with the current average and the same perturbations as at $t = 0$. We use $\Delta t = 0.025$, $Re = 800$, $\mu_2 = 1$, $\mu_1 \Delta x = 0.2$, ($\triangle t$ small enough for stability of EEV1 and EEV2). The results (Supplementary Materials) are consistent with Tests 1 and 2. The EEV1 results improved somewhat but still EEV1 over-diffused while EEV2 did not.

Test #4: Accuracy. We check accuracy on a problem with known exact solution from [15] which has spacial patterns of the Green-Taylor solution, [2], [14], without time decay. Thus, for the true solution the nonlinearity is active for the pressure but not the velocity. For the discrete solution the nonlinearity is active due to discretization and model effects. Define $\widetilde{u}(x,y) = (-\cos x \sin y, +\sin x \cos y)^T$

EV2

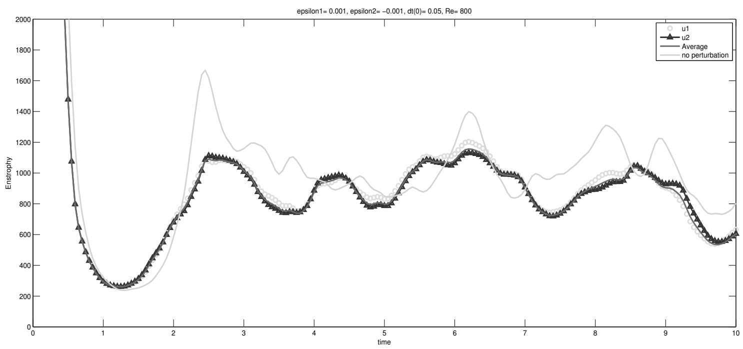

NoEV

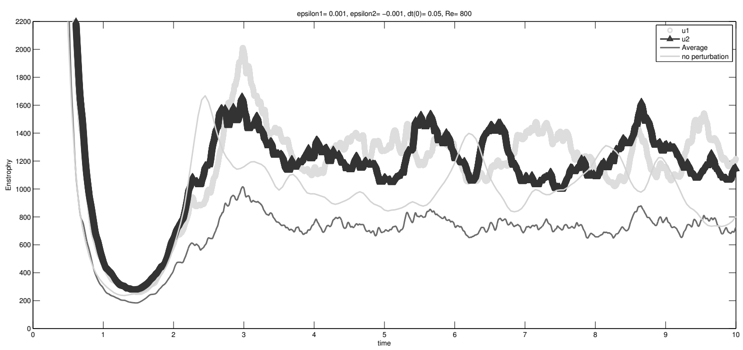

FIGURE 3. Enstrophy, $\nu = 1/800$

$Error$	EV1	EV2
$\lVert\nabla u_1 - \nabla u_{1,h}\rVert_{2,0}$	0.02016440759	0.0162905579
$\lVert\nabla u_2 - \nabla u_{2,h}\rVert_{2,0}$	0.02012253135	0.0162294437
$\lVert\nabla u_{exact} - \nabla u_{ave,h}\rVert_{2,0}$	0.02014346778	0.01625999831
$\lVert\nabla p_1 - \nabla p_{1,h}\rVert_{2,0}$	0.03308893594	0.02667901262
$\lVert\nabla p_2 - \nabla p_{2,h}\rVert_{2,0}$	0.03258390956	0.02619554571

TABLE 1. Re=800, $\Delta t = 0.05, h = 0.1$

and $u(x,y,t) = g(t)\widetilde{u}(x,y)$. Thus

$$u_1 = -g(t)\cos x \sin y, \;\; u_2 = +g(t)\sin x \cos y$$

$$p = -\frac{1}{4}[\cos(2x) + \cos(2y)]g^2(t), \;\; g(t) = \sin(2t).$$

This is an exact solution with body force $f(x,y,t) = \widetilde{u}(x,y)[g'(t) + 2\nu g(t)]$. We compute the solution of EEV1 and EEV2 at $T = 1$ and compute errors.

EV2

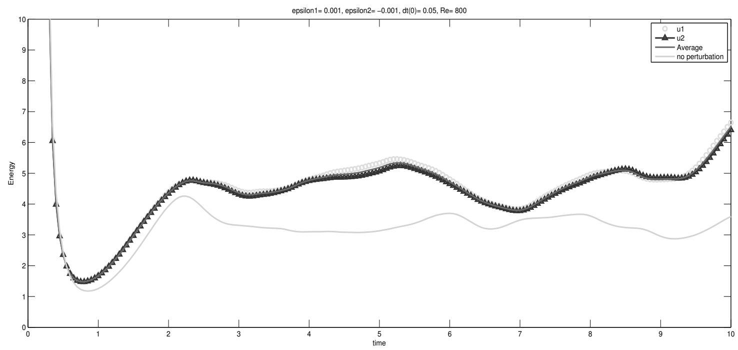

NoEV

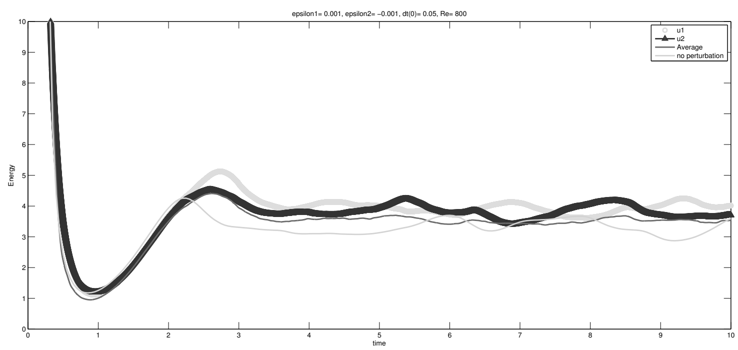

FIGURE 4. Energy, $\nu = 1/800$

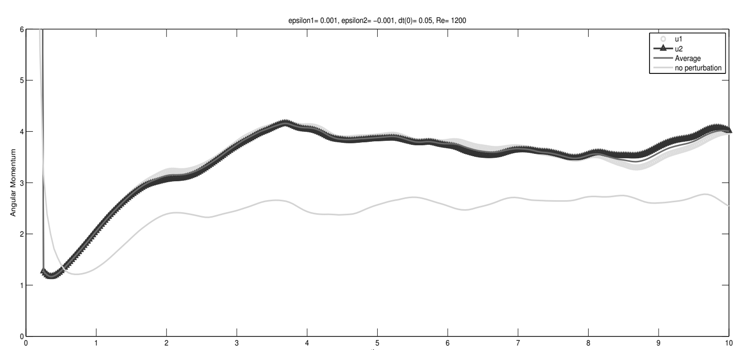

FIGURE 5. EEV2 Angular Momentum, $\nu = 1/1200$

We see acceptable accuracy ($error \sim 10^{-2}$) even on coarse meshes ($\triangle x = 0.1$). This is evidence that the nonlinearity introduced by EEV1&2 is small for smooth

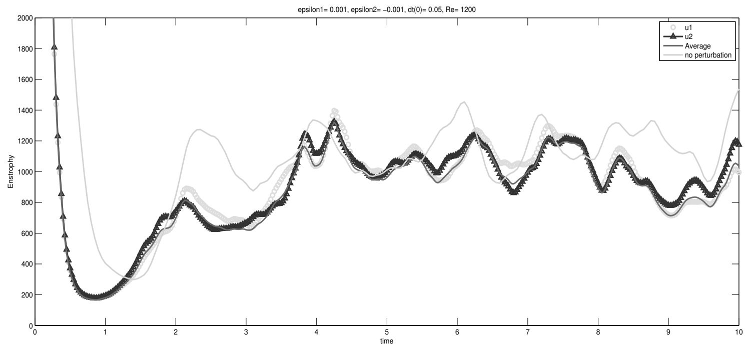

Figure 6. EEV2 Enstrophy, $\nu = 1/1200$

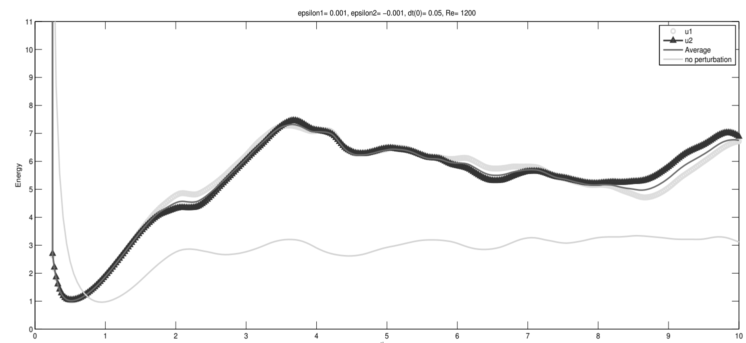

Figure 7. EEV2 Energy, $\nu = 1/1200$

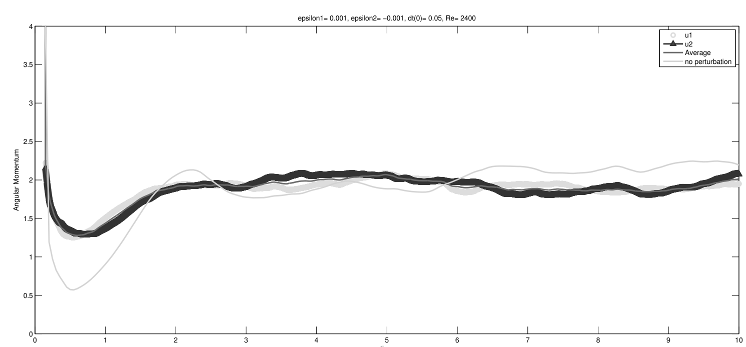

Figure 8. EEV2 Angular Momentum, $\nu = 1/2400$

functions and that the time and space discretization does not introduce significant nonphysical nonlinear effects into the discrete velocity field.

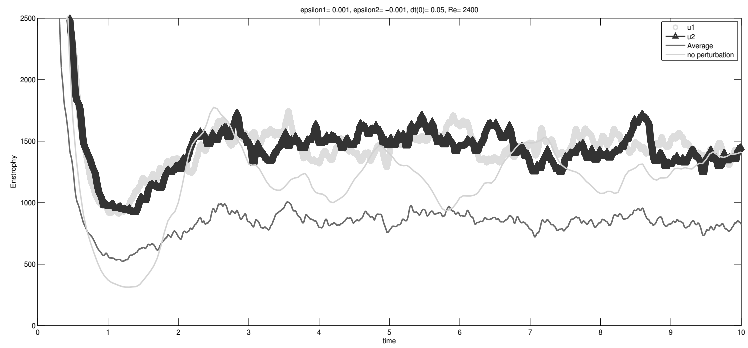

FIGURE 9. EEV2 Enstrophy, $\nu = 1/2400$

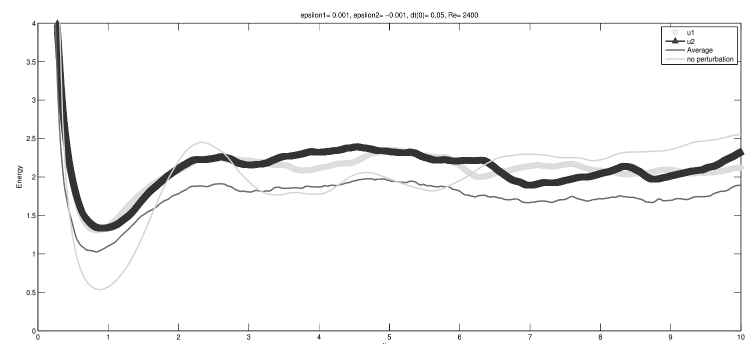

FIGURE 10. EEV2 Energy, $\nu = 1/2400$

$Error$	EV1	EV2
$\|\|\nabla u_1 - \nabla u_{1,h}\|\|_{2,0}$	0.02071888682	0.04244542311
$\|\|\nabla u_2 - \nabla u_{2,h}\|\|_{2,0}$	0.02067566768	0.04229541702
$\|\|\nabla u_{exact} - \nabla u_{ave,h}\|\|_{2,0}$	0.02069727546	0.04237040275
$\|\|\nabla p_1 - \nabla p_{1,h}\|\|_{2,0}$	0.0330861719	0.0274518365
$\|\|\nabla p_2 - \nabla p_{2,h}\|\|_{2,0}$	0.03257960354	0.02697616082

TABLE 2. Re=10,000, $\Delta t = 0.05, h = 0.1$

Test 5: A flow from [18, 23, 4] **with two outlets and a contraction.** The domain is depicted in Figure 15. It has inflow boundary on the LHS and two outflow boundaries (top and RHS) where the do-nothing outflow boundary condition is imposed. Since the boundary conditions do not satisfy $u \cdot \widehat{n} = 0$, the convective form of the nonlinear term $b(u, u, v) = (u \cdot \nabla u, v)$ was used. The body force $f(x, y, t) = 0$ and the perturbed initial conditions are generated as in Test 1. The inflow profile is parabolic $(4 * y * (1 - y), 0)^T$. We take $Re = 1000$ and a

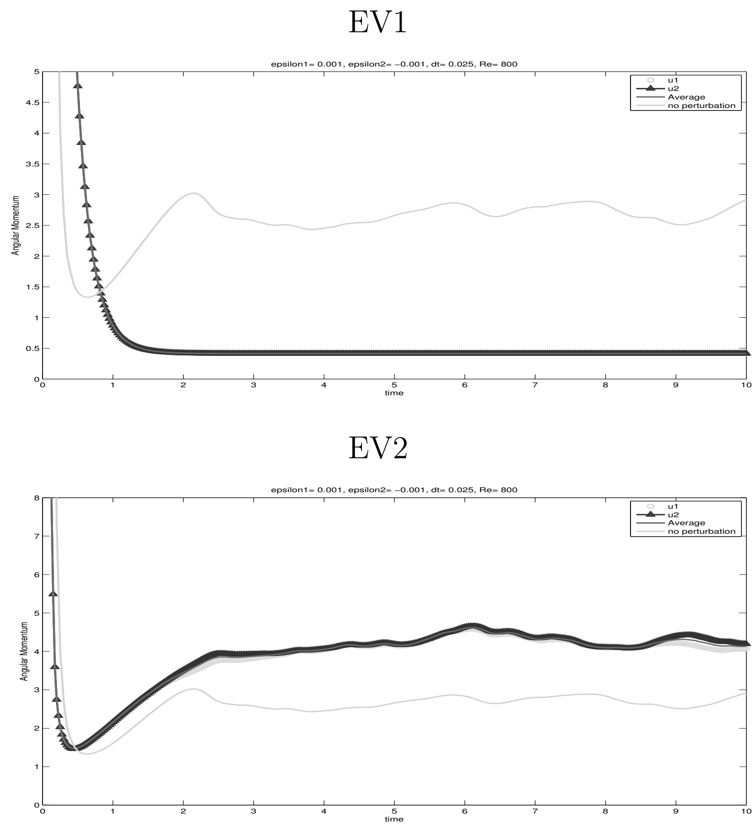

FIGURE 11. Angular Momentum, $\nu = 1/800$

constant timestep $\triangle t = 0.01$. The speed contours at time $T = 4$ for all methods are plotted in Fig. 16. All methods were tested on a coarse mesh which provides $15,133$ total degrees of freedom (DOF). EEV1 and EEV2 stay stable and give solutions matching the pattern shown in [4] and our finer mesh simulation (supplementary materials). NoEV is unstable under the same condition. A comparison of Energy for all three methods is given in Figure 17.

7. Conclusions and Open Questions

While the tests were preliminary, EEV2 outperformed EEV1 in every test. This suggests further study of EEV2. However, it should not be concluded that EEV2 is better in general because the combination of numerical dissipation from the backward Euler time discretization and EEV2 is the active model. This precise combination fits perfectly the needs on controlling the growth due to the lagged term. Changing the time discretization (to a superior high order time discretization) may also change the optimal eddy viscosity parametrization. We also found that, while grad-div stabilization does improve many under-resolved simulations, with EEV2 it added little to solution quality. Further, the high sensitivity of the EEV1

EV1

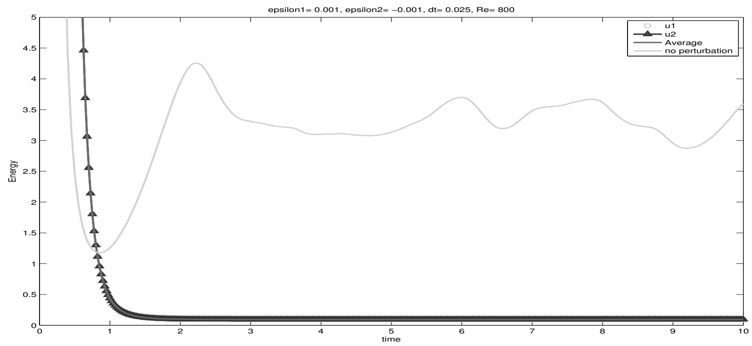

EV2

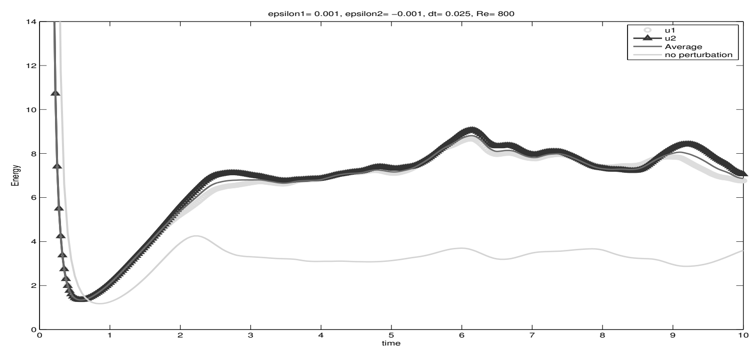

FIGURE 12. Energy, $\nu = 1/800$

results to the parameter choice is only a disadvantage until a good strategy for parameter selection is derived for EEV1, an open problem.

There are many questions open. First, block algorithms for the occurring linear system will determine efficiency and need to be tested. When J is large, the number of realizations per run vs. the number of runs is a compiler issue, needs to be investigated and will vary. The question of how to design an effective, self-adaptive reinitialization strategy is also an important open question. Analytic questions abound concerning existence of solutions to the NSE+EEV2:

$$u_{j,t} + u_j \cdot \nabla u_j - \nu \triangle u_j + \nabla p_j - \nabla \cdot (\mu\tau |u'|^2 \nabla u_j) = f_j(x,t), \text{ in } \Omega,$$
$$\text{where: } u'_j := u_j - < u > \text{ and } \nabla \cdot u_j = 0, \text{ in } \Omega.$$

The closest analog is the (single realization) existence theory in [24] for a model like EEV1. The EEV2 model does not give control over u but rather gives control over

$$\int_0^T \int_\Omega |u_j - \frac{1}{J}\sum_{j=1}^{J} u_j|^2 |\nabla u_j|^2 dx \le C(data, T).$$

EV1

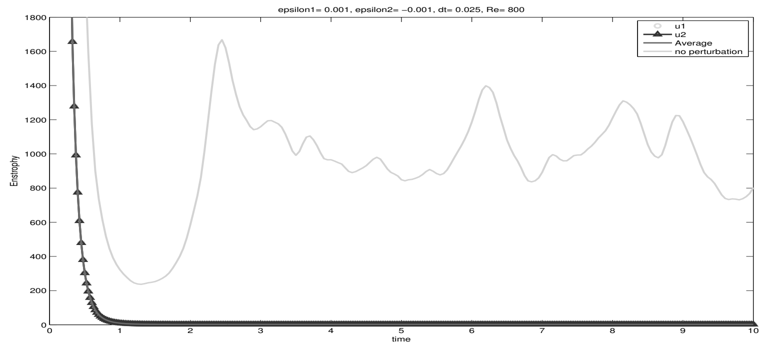

EV2

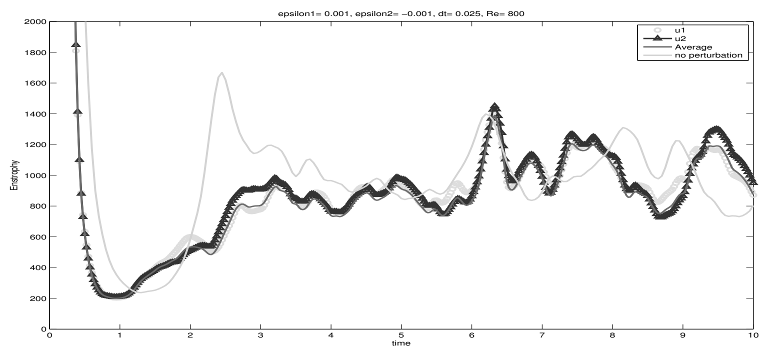

FIGURE 13. Enstrophy, $\nu = 1/800$

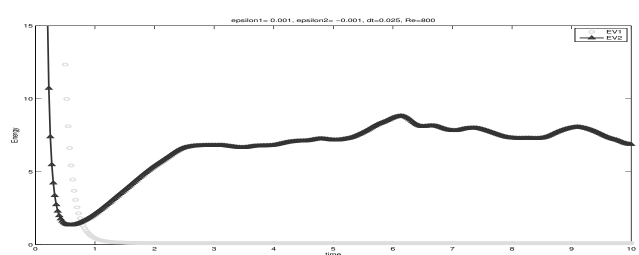

FIGURE 14. Energy: EV1 Vs EV2, $\Delta t = 0.025$, $\nu = 1/800$

Thus, existence is not completely transparent and uniqueness is still a significant challenge.

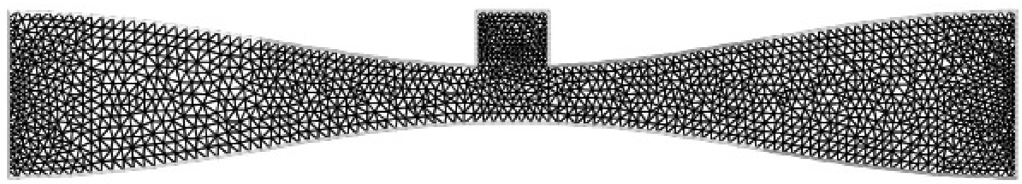

Figure 15. mesh: 15,133 DOF

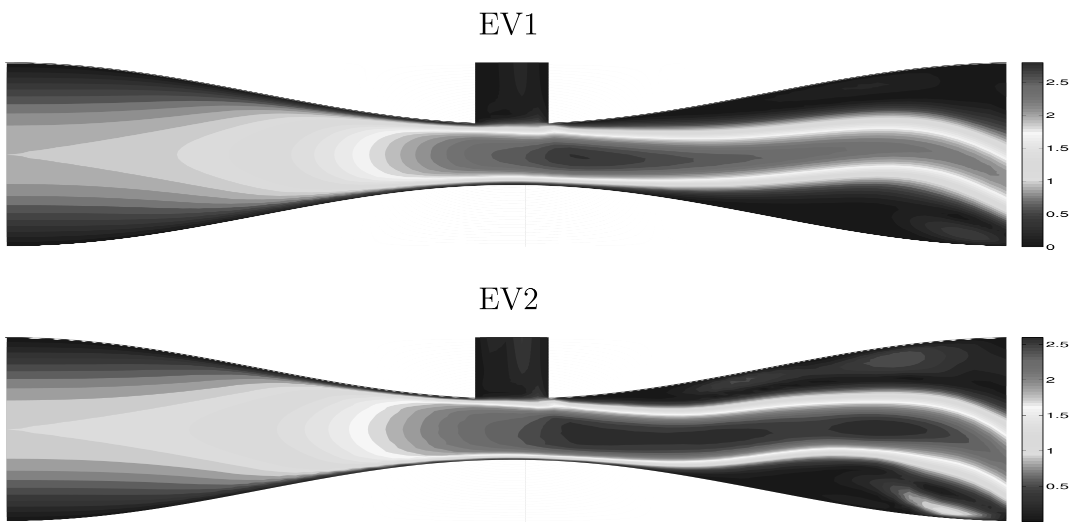

Figure 16. $Re = 1000$, $\Delta t = 0.01$, $T = 4$, $\mu_1 \Delta x = 0.002, \mu_2 = 1$

References

[1] O. Axelsson, *A survey of preconditioned iterative methods for linear systems of algebraic equations*, BIT, 25 (1985), 166-187.

[2] L.C. Berselli, *On the large eddy simulation of the Taylor-Green vortex*, J. Math. Fluid Mech., 7 (2005), S164-S191.

[3] L.C. Berselli, T. Iliescu and W. Layton, *Mathematics of Large Eddy Simulation of Turbulent Flows*, Springer, Berlin, 2006.

[4] A.L. Bowers and L.G. Rebholz, *Numerical study of a regularization model for incompressible flow with deconvolution-based adaptive nonlinear filtering*, CMAME, 258 (2013), 1-12.

[5] S. Brenner and R. Scott, *The Mathematical Theory of Finite Element Methods*, Springer, 3rd edition, 2008.

[6] M. Carney, P. Cunningham, J. Dowling and C. Lee, *Predicting Probability Distributions for Surf Height Using an Ensemble of Mixture Density Networks*, International Conference on Machine Learning, (2005).

[7] M. Case, V. Ervin, A. Linke and L. Rebholz, *A connection between Scott-Vogelius elements and grad-div stabilization*, SINUM 49(2011), 1461-1481.

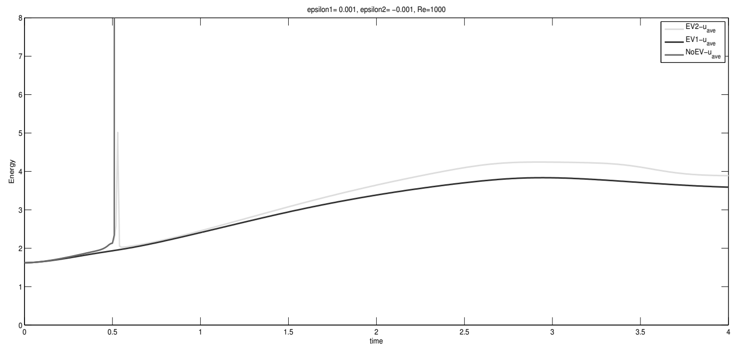

FIGURE 17. Energy:$Re = 1000, \Delta t = 0.01, T = 4, \mu_1 \Delta x = 0.002, \mu_2 = 1$

[8] Y.T. FENG, D.R.J. OWEN AND D. PERIC, *A block conjugate gradient method applied to linear systems with multiple right hand sides*, CMAME 127 (1995), 203-215.

[9] P.F. FISCHER, *Projection techniques for iterative solution of Ax=b with successive right-hand sides*, CMAME, 163, 1998, 193-204.

[10] R.W. FREUND AND M. MALHOTRA, *A block QMR algorithm for non-Hermitian linear systems with multiple right-hand sides*, Linear Algebra and its Applications, 254, 1997, 119-157.

[11] E. GALLOPULOS AND V. SIMONCINI, *Convergence of BLOCK GMRES and matrix polynomials*, Lin. Alg. Appl., 247 (1996), 97-119.

[12] J.D. GIRALDO AND S.G. GARCÍA GALIANO, *Building hazard maps of extreme daily rainy events from PDF ensemble, via REA method, on Senegal River Basin*, Hydrology and Earth System Sciences, 15 (2011), 3605-3615.

[13] M.D. GUNZBURGER, *Finite Element Methods for Viscous Incompressible Flows - A Guide to Theory, Practices, and Algorithms*, Academic Press, (1989).

[14] A.E. GREEN AND G.I. TAYLOR, *Mechanism of the production of small eddies from larger ones*, Proc. Royal Soc. A., 158 (1937), 499-521.

[15] J.L. GUERMOND AND L. QUARTAPELLE, *On stability and convergence of projection methods based on pressure Poisson equation*, IJNMF, 26 (1998), 1039-1053.

[16] T.M. HAMILL, J.S. WHITAKER, M. FIORINO, S.E. KOCH AND S.J. LORD, *Increasing NOAA's computational capacity to improve global forecast modeling*, NOAA White Paper, 19 July 2010.

[17] F. HECHT AND O. PIRONNEAU, *FreeFEM++*, http://www.freefem.org.

[18] J. HEYWOOD, R. RANNACHER AND S. TUREK, *Artificial boundaries and flux and pressure conditions for the incompressible Navier-Stokes equations*, IJNMF, 22 (1996), 325-352.

[19] T.J.R. HUGHES, A.A. OBERAI AND L. MAZZEI, *Large eddy simulation of turbulent channel flows by the variational multiscale method*, Phys. Fluids., 13 (2001), 1784-1799.

[20] T. ILIESCU AND W. LAYTON, *Approximating the Larger Eddies in Fluid Motion III: the Boussinesq Model for Turbulent Fluctuations*, An. St. Univ. "Al. I. Cuza", vol. 44, (1998), 245-261.

[21] N. JIANG AND W. LAYTON, *An algorithm for fast calculation of flow ensembles*, submitted, April 2013, available at: http://www.mathematics.pitt.edu/sites/default/files/research-pdfs/ensemble2April2013.pdf.

[22] V. JOHN, *Large Eddy Simulation of Turbulent Incompressible Flows. Analytical and Numerical Results for a Class of LES Models*, Lecture Notes in Computational Science and Engineering 34, Springer-Verlag, Berlin, 2004

[23] P. KUBERRY, A. LARIOS, L. REBHOLZ AND N. WILSON, *Numerical approximation of the Voigt regularization for incompressible Navier-Stokes and magnetohydrodynamic flows*, Comput. Math. Appl., 64 (8) (2012), 2647-2662.

[24] W. Layton and R. Lewandowski, *Analysis of an eddy viscosity model for large eddy simulation of turbulent flows*, J. Math. Fluid Mechanics, 2 (2002), 374-399.
[25] O.P. Le Maitre and O.M. Kino, *Spectral methods for uncertainty quantification*, Springer, Berlin, 2010.
[26] O.P. Le Maitre, O.M. Kino, H. Najm and R. Ghanem, *A stochastic projection method for fluid flow, I. Basic Formulation*, JCP, 173 (2001), 481-511.
[27] W. Layton and L. Tobiska, *A Two-Level Method with Backtracking for the Navier–Stokes Equations*, SINUM, 35 (1998), pp. 2035-2054.
[28] M. Leutbecher and T.N. Palmer, *Ensemble forecasting*, JCP, 227 (2008), 3515-3539.
[29] R. Lewandowski, *The mathematical analysis of the coupling of a turbulent kinetic energy equation to the Navier-Stokes equation with an eddy viscosity*, Nonlinear Analysis, 28 (1997), 393-417.
[30] J.M. Lewis, *Roots of ensemble forecasting*, Monthly Weather Rev., 133 (2005), 1865-1885.
[31] W.J. Martin and M. Xue, *Initial condition sensitivity analysis of a mesoscale forecast using very-large ensembles*, Mon. Wea. Rev., 134 (2006), 192-207.
[32] D.P. O'Leary, *The block conjugate gradient algorithm and related methods*, Linear Algebra and its Applications, 29 (1980), 293–322,
[33] M. Olshanskii and A. Reusken, *Grad-Div stabilization for the Stokes equations,* Math. of Comp. 73 (2004) 1699-1718.
[34] P. Sagaut, *Large eddy simulation for Incompressible flows*, Springer, Berlin, 2001.
[35] D.J. Stensrud, *Parameterization schemes: Keys to numerical weather prediction models*, Cambridge U. Press, 2009.
[36] G.I. Taylor, *On decay of vortices in a viscous fluid*, Phil. Mag., 46 (1923), 671-674.
[37] Z. Toth and E. Kalney, *Ensemble forecasting at NMC: The generation of perturbations*, Bull. Amer. Meteor. Soc., 74 (1993), 2317-2330.